43rd AIAA/ASME/SAE/ASEE Joint Propulsion Conference & Exhibit
8 - 11 July 2007, Cincinnati, OH

AIAA 2007-5590

Mixing Lengths of Coaxial Jets in a Rocket Combustor Configuration Using Acetone PLIF

S. Alexander Schumaker* and James F. Driscoll†

The University of Michigan, Department of Aerospace Engineering, 1320 Beal Avenue, Ann Arbor, MI 48109

This paper explores the mixing field of non-reacting shear coaxial jets as they apply to rocket fuel injectors; flows characterized by a low-velocity high-density inner jet surrounded by a high-velocity low-density annular jet. Using quantitative acetone PLIF, average and instantaneous mixture fraction fields are obtained while velocity ratio, density ratio and Reynolds number are systematically varied. Using the stoichiometric values of O_2/H_2 and O_2 /CH_4, centerline stoichiometric mixing lengths are determined. These lengths are found to scale with the square root of the inner to outer jet momentum ratio.

Nomenclature

C	Scalar concentration
d	Jet diameter
f	Mixture fraction based on inner jet fluid
L	Centerline mixing length
M	Inner to outer momentum flux ratio $= \rho_i U_i^2/\rho_e U_e^2$
r_u	Inner to outer mean velocity ratio
S	Inner to outer density ratio
T_P	Inner post thickness
u	Jet exit mean velocity
u_{ee}	Entrainment velocity
u'	Turbulent intensity
Δt	Time interval
ρ	Density

Subscript

e	Relative to external jet
i	Relative to inner jet
S	Relative to stoichiometric value
∞	Relative to ambient fluid surrounding jet

I. Introduction

A research effort is underway as part of the NASA CUIP program to provide mixing data to assess and validate NASA Marshall's rocket thrust chamber assembly design codes. This effort has two main components. First, provide a benchmark data set of rocket combustion properties including flame size, standoff distance, mixing fields with and without combustion, and mixing lengths at chamber pressures from 1 to 10 atmospheres for the simple geometry of a coaxial jet injector. Second, extend the understanding of coaxial jets and coaxial jet flames as they apply to rocket injectors. To aid in these goals, a single element gas-gas coaxial injector in a rocket combustion chamber is utilized due to the number of advantages

*Graduate Student, Aerospace Engineering Department, The University of Michigan, Ann Arbor, MI, Member
†Professor, Aerospace Engineering Department, The University of Michigan, Ann Arbor, MI, Fellow

it provides for both model validation and studies of turbulent shear mixing over a multiphase flow. First, the boundary conditions are well known and can be modeled as fully developed pipe flow. Second, gas-gas allows the combustion and mixing models to be assessed without assuming a spray distribution. In addition, gas-gas allows the use of Planar Laser Induced Fluorescence (PLIF) techniques. Last, by closely matching the reacting and non-reacting test conditions the effects of heat release and fluid dynamic mixing can be separated, allowing the mixing and combustion models to be determined separately. As a first step in this effort, the non-reacting mixing field is studied.

The simple geometry of a turbulent coaxial jet has made it a staple in applications where two fluid streams need to be mixed. Applications include fuel injectors, pumps, cooling systems, premixed flame burners and jet engines. When used as fuel injectors in liquid propellent rocket engines, coaxial jets are characterized by a low-velocity high-density inner jet surrounded by a high-velocity low-density annular jet. These characteristics result in large density ratios, $S = 16$ GO_2/GH_2 and $S = 2$ GO_2/GCH_4, and small velocity ratios, $r_u < 1$.

Early work on coaxial jets focused on the velocity field and turbulent statistics in the potential core region for uniform density flows. Champagne and Wygnanski[1] used a hot-wire anemometer to measure mean velocities, turbulent intensities and shear stresses at two area ratios and r_u values ranging from 0.1 to ∞. Results indicate that the far field has a self preserving nature and that r_u is the most important independent variable in determining inner jet potential core length, while the secondary core lengths are largely independent of r_u. Durão & Whitelaw[2] and Ribeiro & Whitelaw[3] studied $r_u < 1$ and $r_u = 1$ respectively and for both cases showed that the coaxial jet reached a self-preserving state faster than a singe jet. Also the importance of the injector post thickness was noted as the $r_u \rightarrow 1$. This corresponds to a change in the mixing layer from a shear like instability to a wake like instability.[4] Ribeiro & Whitelaw[5] also showed that swirling of the outer jet for r_u ranging from 0.65 to 1.5 causes a decrease in the distance to self-preservation.

While these papers investigated the dependence of mixing on r_u and the area ratio, the first work on the structure of the mixing layers was performed by Ko and Kwan.[6,7] Using pressure measurement, hot wire, and microphone spectra in air-air coaxial jets it was shown that two separate vortical mixing zones exist; the first between the inner jet and the secondary outer jet and the second between the outer jet and the ambient fluid. The results indicate the growth, decay and dominance of these layers is governed by r_u. Dahm et al.,[4] using a two-color PLIF technique in water jets, revealed a number of regimes based on the structures of the vortices which depended on not only r_u, but to a lesser extent on the velocity difference over the mixing layer. For $r_u < 1$ results indicate the secondary mixing layer is dominant and as r_u decreases the degree of coupling between the two mixing layers increases.

The mentioned studies illustrate the importance of the r_u on the near field mixing, but the effect of density ratio, S, is ignored due to the use of uniform density coaxial jets. Favre-Marinet et al.[8] and Favre-Marinet & Camano[9] studied SF_6/helium, air/helium, and air/air jets with S values of 35.7, 7.14, and 1 for r_u values between 0.01 and 0.33. Results show that the density effects on inner jet potential core are taken into account by inner to outer jet momentum flux ratio, M, and not the r_u and S separately.

In most situations, combustion reactions using coaxial jets in rocket combustors are diffusion controlled, signifying the reaction is controlled by the turbulent mixing of the jet. In this type of reaction, the flame sits on the stoichiometric contour. Hence, one method to predict the flame length is to model the centerline stoichiometric mixing distance, L_S, of the non-reacting jet and then add in the effect of heat release. Such a method has been demonstrated by Tacina and Dahm[10] and Dahm[11] for reacting turbulent jets and shear layers respectively. To apply to coaxial jet flames, a model for the centerline stoichiometric mixing distance is needed for the non-reacting case.

Three possible models are presented in the literature. The first by Dahm and Mayman[12] uses momentum conservation and assumes that the jet has reached a self preserving state. The second, by Murakami and Papamoschou[13] uses the turbulent shear layer equation derived by Dimotakis[14] to predict the growth of the inner and outer shear layers and from these growth rates calculates the length of the potential core. Last, Villermaux and Rehab[15] and Rehab et al.[16] use a simple mass entrainment argument.

In the current paper average and instantaneous mixture faction fields and stoichiometric mixing lengths are presented for a number of non-reacting coaxial jets obtained using quantitative acetone PLIF. The effects of density ratio, velocity ratio, diameter ratio, confinement and Reynolds number on the stoichiometric mixing lengths are explored. Results are compared with the mass entrainment model of Villermaux and Rehab.[15]

II. Experimental Setup

II.A. Experimental Apparatus

Experiments were conducted in The Michigan Single Element Injector Experiment shown in Fig. 1 and previously described by the authors.[17] This facility is a laboratory scale rocket engine with optical access. The design and sizing of the rocket is based on work done at Penn State and NASA Marshall.[18–20] The rocket is of a modular design which allows a window section to be moved to any location in the combustion chamber and for the combustion chamber length to be varied by the addition or removal of spacer sections. The 50.8mm x 50.8mm square chamber with rounded corners allows chamber pressures up to 10 atmospheres.

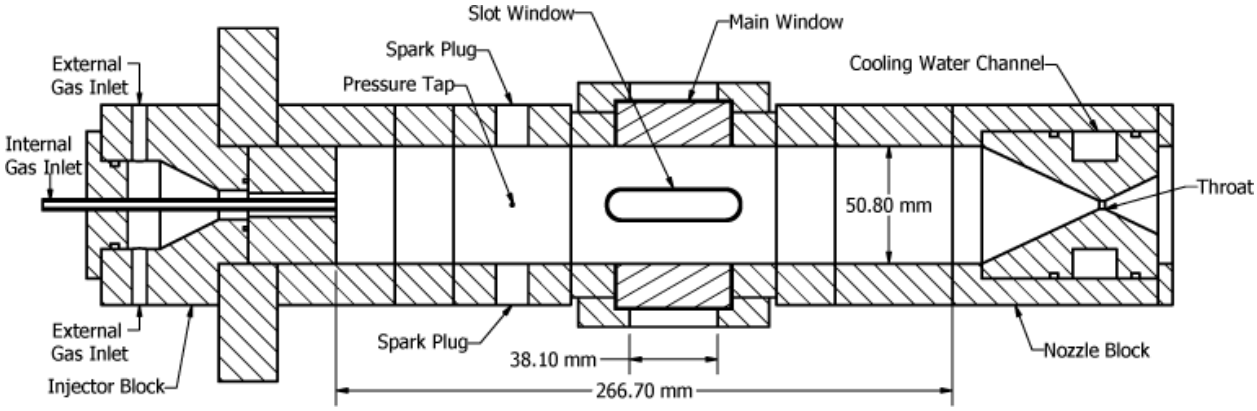

Figure 1. Schematic of the Michigan Single Element Injector Experiment

Data was obtained in a number of experimental configurations. Cases taken at atmospheric pressure were obtained by removing the nozzle block and leaving the chamber side walls. Such a configuration was used because it is more representative of the confined reacting flow field of interest and because the confinement leads to an ambient gas that is the combination of the injector gases. This creates an ambient fluid that is also seeded with acetone allowing both the inner and outer mixing layers to be viewed and evaluated. However to understand the effect of this confinement, results were also obtained with the chamber side walls removed. Jet Reynolds number effect was investigated by raising the chamber pressure and hence the Reynolds number. For these cases, the nozzle block was used with a throat diameter of 2.16mm. In addition, the effect of diameter ratio was investigated using three injector configurations. Characteristic dimensions for the three injectors are listed in Table 1.

Table 1. Injector configurations

Injector	d_e, mm	d_i, mm	T_P, mm	$\frac{d_e}{d_i}$
1	7.52	3.00	0.89	2.51
2	7.52	3.66	0.54	2.05
3	10.03	3.00	0.89	3.34

For the current effort, the propellent delivery system was modified to flow acetone-seeded air from the inner jet and helium, hydrogen or methane from the external jet. The acetone-seeded air was produced by bubbling a known flow rate of air through acetone and combining it with another known flow rate of air, allowing any acetone concentration, up to the saturation value, to be delivered to the inner jet. All flow metering was accomplished via choked orifices.

II.B. Quantitative Acetone PLIF

The use of acetone as a flow tracer is described by Lozano et al.,[21] Yuen et al.,[22] and Thurber and Hanson.[23] An illustration of the quantitative acetone PLIF setup is shown in Fig. 2. Acetone fluorescence was excited at a wavelength of 266nm. Fluorescence was produced by taking the second harmonic, 532nm, from a Spectra-Physics GCR-130 Nd-YAG laser and using an external BBO doubling crystal. The 266nm laser beam was

then split sending 90 percent of the energy into the sheet forming optics and 10 percent into a secondary measurement. The fluorescence from the test section was collected between 400nm and 700nm on a scientific grade CCD (Sony XCD-710) using a Nikon f/1.4 50mm Nikkor lens. No filter was used since the BK7 glass lens effectively blocked the 266nm light. Note that air was always used as the inner jet gas allowing the oxygen to quench the acetone phosphorescence making the use of a gated camera unnecessary. The second beam path was then further split using a glass flat sending beams to a photodiode (Thorlabs DET10A) and through a reference cell. The reference cell was plumbed inline with the inner jet allowing the acetone-seeded air to pass through the reference cell right before being injected into the test section. A photo-multiplier tube (Hamamatsu R636-10) was used to measure the fluorescence of the pure acetone-air mixture. This measurement was then used to normalize the test section fluorescence and to correct for shot-to-shot power variations. A second photodiode was placed at the beam exit from the reference cell and used in combination with the first photodiode to perform an absorbtion spectroscopy measurement from which the acetone mole fraction was calculated, allowing the conversion from concentration to mixture fraction. Corrections for sheet non-uniformity were made by normalizing each image by an image of the sheet taken with the test section filled with an uniform acetone-air mixture. In addition, corrections for background scatter, dark noise, and absorbtion were made as outlined by Cruyningen et al.[24] and by Clemens.[25] A nominal 18 percent by volume acetone seeding was used for all atmospheric cases. Acetone seeding was adjusted at other chamber pressures to maintain the same fluorescence signal level.

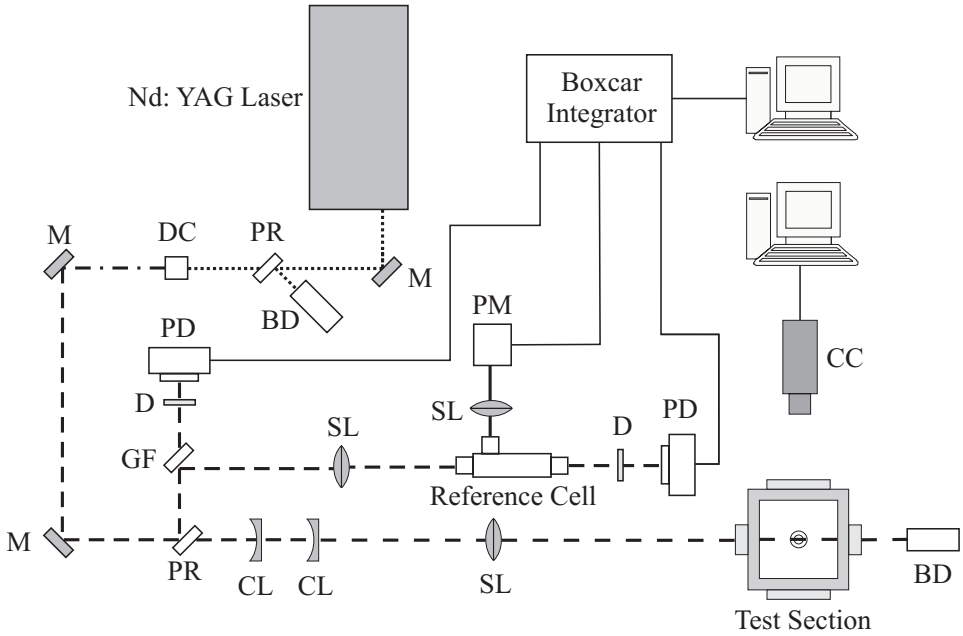

Figure 2. Laser and optical setup for quantitative acetone PlIF measurements. BD - beam dump, CC - CCD camera, CL - cylindrical lens, D - diffuser, GF - glass flat, M - mirror, DC - doubling crystal, PD - photodiode, PM - photo-multiplier tube, PR - partial reflector, SL - spherical lens. $(\cdots)$ **- 532 nm ,** $(- - -)$ **- 266 nm**

II.C. Experimental Conditions

Experimental test conditions were divided into eleven data groups. Data groups were defined as test conditions with the same density ratio, diameter ratio, rocket configuration and chamber pressure, but a varying velocity ratio. These data groups are listed in Table 2 along with their governing non-dimensional parameters, external jet density and velocity-range and comments on what makes each group unique. The Reynolds number Re is based on a theoretical jet with external jet fluid properties and a velocity giving it the same total momentum flux as the actual coaxial jet,

$$Re = \frac{\rho_e d_e}{\mu_e} u_e \left[1 + \frac{1 - M^{-1}}{M^{-1} \left(\frac{d_e}{d_i} \right)^2} \right]^{1/2} . \tag{1}$$

Table 2. Experimental data groups

Data Group	$\frac{\rho_i}{\rho_e}$	$\frac{d_e}{d_i}$	$\frac{u_i}{u_e}$	$\rho_e, kg/s$	$u_e, m/s$	Re	Comments
G1	8.46	2.51	0.1-0.9	0.163	42.4-71.6	3,540-4,110	
G2	8.49	2.51	0.2-0.6	0.163	37.1-112	2,650-6,550	u_i held constant
G3	8.48	2.51	0.2-0.4	0.163	81.7	4,810-5,200	u_e held constant
G4	2.16	2.51	0.2-0.4	0.644	56.6-115	26,200-45,000	Outer jet gas CH_4
G5	16.9	2.51	0.1-0.9	0.0817	25.2-227	2,940-14,300	Outer jet gas H_2
G6	8.40	2.05	0.2-0.4	0.163	63.8-128	4,070-7,200	
G7	8.44	3.34	0.2-0.9	0.163	42.3-82.2	4,090-6,610	
G8	8.53	2.51	0.1-0.9	0.163	42.4-71.2	3,540-4,090	G1 except unconfined
G9	17.0	2.51	0.1-0.9	0.0817	25.2-227	2,970-14,200	G5 except unconfined
G10	7.57	2.51	0.2-0.9	0.627	43.8-69.3	13,900-15,300	Pressure of 3.76 atm
G11	7.49	2.51	0.2-0.9	0.895	46.0-71.6	21,000-23,000	Pressure of 5.40 atm

With these data groups three inner/outer gas combinations were examined, air/helium, air/H_2, and air/CH_4 producing density ratios of 8.5, 17, and 2.2 respectively. Note that the density ratio changes case-to-case for the same gas combination due to changes in the acetone seeding. In addition to density ratios, three diameter ratios, 2.51, 2.05, and 3.34 were studied. Lastly, the effects of confinement, G8 and G9, and increasing Reynolds number, G10 and G11, were examined.

III. Model Analysis

For coaxial jets in the context of fuel injectors in rocket engines, the important dependent variable is the stoichiometric centerline mixing distance L_S since it sets the flame length in a diffusion controlled reaction. By definition, the stoichiometric contour has to sit outside of the potential core and hence beyond the near field mixing region. However, for the oxidizer/fuel combinations of interest, O_2/H_2 and O_2/CH_4, the stoichiometric mixture fraction f_S is relatively large, 0.89 and 0.80 respectively, resulting in a L_S that lies close to the end of the inner potential core. This results in the stoichiometric contour residing in the intermediate mixing zone located between the near and far fields. Hence, to model the stoichiometric mixing length a near or far field argument must be extended to this region. A schematic of the near field mixing layers and the stoichiometric contour is shown in Fig. 3.

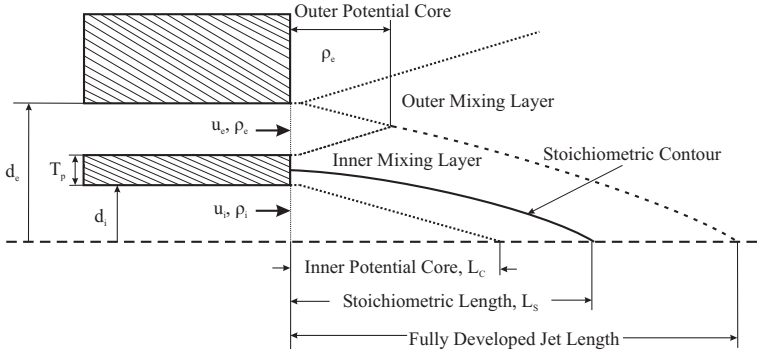

Figure 3. Schematic of coaxial jet injector and the near to intermediate field mixing layers

One approach to predicting L_S, based on far field analysis, uses conservation of momentum and assumes the coaxial jet has reached a self-preserving state. Using this approach Dahm and Mayman[12] are able to write L_S as

$$\frac{L_S}{d_i} = \frac{4.75 f_S^{-1}(\rho_i/\rho_\infty)^{1/2}}{\left[1 + (\frac{1}{r_u S})\left(\frac{d_e^2 - d_i^2}{d_i^2}\right)\right]^{1/2}}. \tag{2}$$

Results indicate that for the present configurations that L_S is between $2d_i$ and $16d_i$ where as work by Warda et al.[26] show for similar velocity ratios in air/air coaxial jets that self-similarity had not been reached by $25d_i$, making the far field assumption questionable for the current configuration. In addition, Eq. 2 assumes that fluid must be entrained from the ambient to reach a stoichiometric value. In the current effort all cases are run fuel-rich making entrainment from the ambient unnecessary and actual harmful to mixing since the ambient fluid is not pure fuel.

A second approach to modeling L_S is to treat the near field inner and outer mixing layers as turbulent planar shear layers and use the shear layer growth equation derived by Dimotakis.[14] Using this approach Murakami and Papamoschou[13] are able to write L_S as

$$\frac{L_S}{d_i} = \frac{0.14(1 - r_u^{-1})(1 + S^{-1})^{1/2}}{1 + M^{-1/2}} + \{11.2(f_S^{-1} - 1)S^{-1}(d_e/d_i)r_u\}^{1/3}. \tag{3}$$

As the velocity ratio across a planner shear layer approaches one the shear layer growth rate approaches zero. However in coaxial jets as the velocity ratio approaches one the shear-like mixing layers transition into wake-like mixing layers as shown by Dahm et al.,[4] which results in a shorter stoichiometric mixing length then predicted by shear layer growth rates at higher velocity ratios.

An additional method to predict the stoichiometric mixing length is to make a global mass entrainment argument as done by Villermaux and Rehab.[15] During any time interval, Δt, the amount of the scalar injected by the center jet is $\frac{1}{4}\pi d_i^2 u_i C_O \Delta t$ where C_O is the scalar concentration at the jet exit. If steady state is assumed, each isoconcentration surface, including the stoichiometric contour, is crossed at an entrainment velocity, u_{ee}. For a coaxial jet, the shape of this contour is somewhere between a cone and a cylinder. Assuming a cylindrical shape, the quantity of scalar injected during time Δt is diluted in a volume $\pi d_i L_S u_{ee} \Delta t$ down to the stoichiometric concentration C_S. This allows the scalar mass balance to be written as

$$d_i^2 u_i \Delta t C_O \sim d_i L_S u_{ee} \Delta t C_S. \tag{4}$$

Using Hill's[27] results for variable density turbulent jets and the entrainment hypothesis that u_{ee} is proportional to the turbulent intensity u', u_{ee} can be written as

$$u_{ee} \sim S^{-1/2} u'. \tag{5}$$

For the case where $r_u << 1$, Dahm et al.[4] and Villermaux and Rehab[15] showed that the outer jet is dominate, hence $u' \sim u_e$. The scalar mass balance can then be rearranged to solve for the stoichiometric mixing length in terms of the momentum ratio

$$\frac{L_S}{d_i} \sim r_u S^{1/2} \frac{C_O}{C_S} = M^{1/2} \frac{C_O}{C_S}. \tag{6}$$

Assuming constant pressure and temperature the concentration ratio can be rewritten in terms of the stoichiometric mixture fraction

$$\frac{L_S}{d_i} \sim M^{1/2}(S(f_S^{-1} - 1) + 1) \tag{7}$$

IV. Results and Discussion

Average and instantaneous mixture fraction fields for non-reacting coaxial jets are presented and discussed in this section. From these images, centerline stoichiometric mixing lengths L_S are determined and plotted to assess the effect of velocity ratio r_u, density ratio S, confinement, and Reynolds number. While the test conditions outlined in Table 2 use acetone seeded air as the center jet fluid, the stoichiometric mixture fraction was defined based on using pure oxygen as the oxidizer. This was done so direct comparison with reacting O_2/H_2 and O_2/CH_4 coaxial jets could be made. Therefore, a stoichiometric mixture fraction value of 0.89 for H_2 cases and 0.80 for CH_4 cases was used. For helium cases, the stoichiometric mixture fraction

value of hydrogen was used. In mixture fraction images, it should be noted that the background mixture fraction is the result of the complete mixing of the coaxial jet and consequently changes from case-to-case. Since all cases are run fuel rich, no entrainment from the ambient fluid is needed. In fact, since the ambient fluid is a mixture of fuel and acetone seeded air entrainment from the ambient fluid increases L_S.

IV.A. Velocity Ratio

To test the dependence of L_S on r_u, data groups G1, G2, and G3 are plotted in Fig. 4(a). These data groups correspond to air/helium jets at a fixed diameter ratio, however they differ in the manner in which r_u is varied. In G1 both u_i and u_e are varied while in G2 u_i is held constant and u_e varied. In G3 u_e is held constant while u_i is varied. As evident by Fig. 4(a) L_S scales linearly with r_u. This however leaves the question of how far beyond the potential core can this scaling be applied. Centerline mixture fraction profiles of data group G1, Fig. 4(b), provide some insight. These profiles are characterized by a flat region, associated with the potential core, followed by a near linear decrease. At some downstream distance this linear decrease stops and the profile begins to level off. This leveling off is due to the combining of the inner and outer mixing layers resulting in significant amounts of entrained ambient fluid being mixed with the inner jet fluid and a loss of the near field mixing structure and thus a loss of the near field r_u scaling.

Average and instantaneous mixture fraction fields of air/H_2 coaxial jets, data group G5, are shown in Fig. 8. In these images it is observed that the spreading of the outer mixing layer is delayed 2-3 inner jet diameters. This delay can be explained by the combination of a possible laminar boundary layer profile at the jet exit in the annular jet and a static pressure gradient perpendicular to the outer jet velocity vector which also causes the bending in of the outer jet near the jet exit.

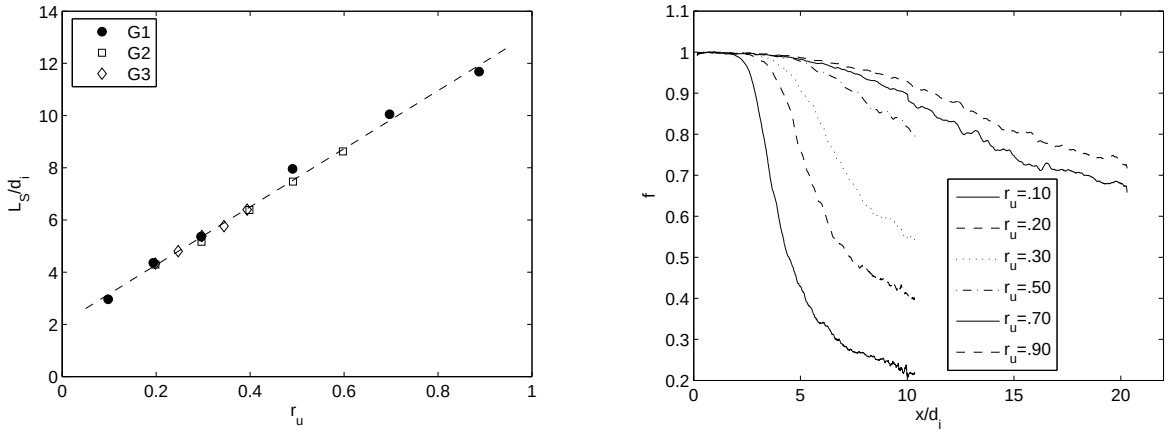

(a) (b)

Figure 4. a) Velocity ratio scaling. b) Centerline mixture fraction profiles

IV.B. Density Ratio

Coaxial jets used as rocket injectors are characterized by their large density ratios. Using data groups G1-air/He, G4-air/CH_4, and G5-air/H_2, Fig. 5(a) shows that scaling by the r_u alone does not account for varying S jets. To account for varying S the mass entrainment model of Villermaux and Rehab[15] can be used as shown in Fig. 5(b). These results indicate that for variable density coaxial jets L_S can be scaled using the square root of the inner to outer momentum ratio M. However, the two longest L_S values from Fig. 5(b) deviate from the above scaling. These points correspond to an air/H_2 coaxial jet with velocity ratios of 0.70 and 0.90. If this deviation was caused by ambient fluid entrainment as previously discussed, the model should under predict L_S and not over predict it as is the case. One hypotheses for this behavior is that the inner and outer mixing layers transitioned from shear-like to wake-like as described by Dahm et al.[4] in an air/air coaxial jet for $r_u = 1$. However, due to the large S and the relatively thick inner post, transition will occur at a much lower velocity ratio value in the current situation then found by Dahm et al.[4] Also in the derivation of the momentum ratio scaling the outer jet was assumed to be dominate, however with such a large S and high r_u values this assumption starts to breakdown. In addition, buoyancy effects

become important as L_S becomes longer and the density of the outer fluid increases. An increase in the ambient fluid density occurs due to the confinement and the decrease of u_e which results in a lower mass flow rate.

Average and instantaneous mixture fraction fields for the the three density ratios at $r_u = 0.30$ are provided in Fig. 9. Note that even with a lower stoichiometric mixture fraction the smaller S value of the air/CH_4 case produces the smallest L_S.

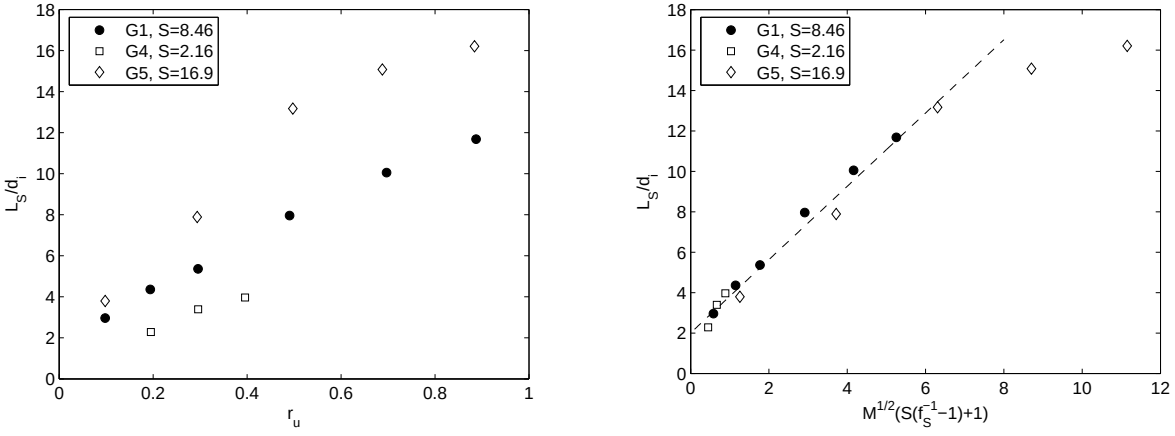

(a) (b)

Figure 5. a) Velocity ratio scaling with varying density ratio jets. b) Momentum ratio scaling with varying density ratio jets

IV.C. Diameter Ratio and Confinement

In addition to experimentally investigating the velocity and density ratios, the effects of diameter ratio and confinement were explored. Figure 6(a) shows data for the three injectors listed in Table 1. Data groups G1, G6, and G7 correspond to injectors 1, 2, and 3 respectively. Injector 1 is the baseline case. Injector 2 was designed to test the effect of inner post thickness, while Injector 3 was designed to test the effect of the outer diameter. Results show these parameters had no effect on the stoichiometric mixing length over the r_u range, 0.20-0.90, and S value, 8.43, examined.

To ensure that the chamber side walls were not creating large recirculation zones that effected mixing lengths, the walls were obtained. These results are plotted in Fig. 6(b) where data group G1 and C5 are the confined air/He and air/H_2 cases respectively. Results show excellent correlation between unconfined and confined cases except at the $air/H2$ cases with r_u =0.70 and 0.90. The same effects discussed in Section IV.B are occurring, except the differences between the confined and unconfined cases can be attributed to the difference in ambient fluid. The confined cases have a larger L_S then the unconfined since in the confined case acetone seeded air is being entrained while in the unconfined case room air is. Since the acetone PLIF system cannot tell where the acetone seeded air originated, the L_S of the confined case is artificially lengthened.

IV.D. Reynolds Number

Coaxial jets used as rocket injectors are not only characterized by their large density ratios, but also by their large Reynolds numbers, as defined in Eq. 1. The effect of increasing Reynolds number was explored by obtaining experimental results at chamber pressures of 3.76 and 5.40 atmospheres. These pressures raised the Reynolds number from 3,500-4,100 at atmospheric to 14,000-15,000 at 3.76atm and 21,000-23,000 at 5.40atm. Results are plotted in Fig. 7. Results show an increase in L_S with the Reynolds number for velocity ratios larger than 0.20. The increase in L_S becomes larger as the velocity ratio increases. These results can be explained by looking at the mixture fraction fields for velocity ratio values of 0.20, Fig. 10, and 0.90, Fig. 11. These images show that as the Reynolds number is increased the outer mixing layer starts to grow closer to the jet exit resulting in a shorter external jet length. For a velocity ratio value of 0.20 the stoichiometric mixing length is still short enough compared to the external jet to inhibit ambient entrainment to the centerline. However as the velocity ratio increases the external jet becomes too short

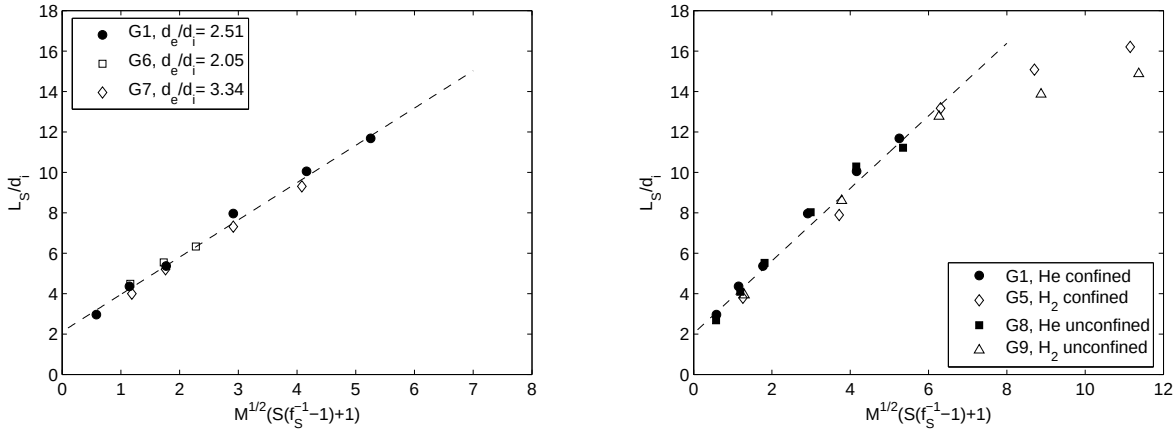

(a) (b)

Figure 6. a) Effects of diameter ratio on stoichiometric mixing lengths. b) Effects of confinement on stoichiometric mixing lengths

and ambient entrainment to the centerline becomes significant, increasing the mixing length. As previously discussed buoyancy effects maybe important at large values of L_S. Additional work is needed to understand buoyancy effects on L_S and when buoyancy effects becomes significant.

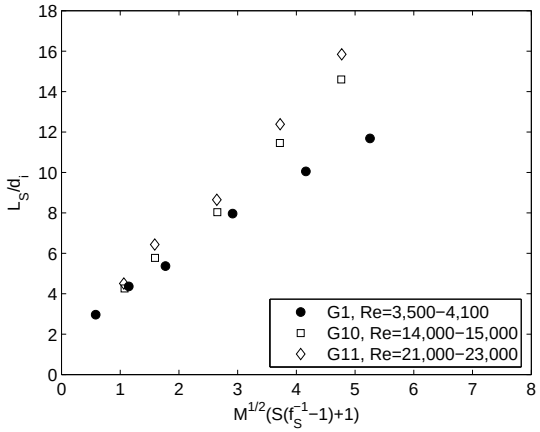

Figure 7. Effect of jet Reynolds number on stoichiometric mixing lengths

V. Conclusions

Quantitative acetone PLIF has been used to obtain mixture fraction fields of non-reacting coaxial jets as they relate to rocket injectors; flows characterized by a low-velocity high-density inner jet surrounded by a high-velocity low-density annular jet. Using the stoichiometric values of O_2/H_2 and O_2/CH_4, centerline stoichiometric mixing lengths were determined. It was found that the near field scaling by Villermaux and Rehab,[15] based on mass entrainment, can be extended to the centerline stoichiometric mixing lengths and beyond for most cases. This results in the stoichiometric mixing length being proportional to the square root of the inner to outer jet momentum ratio. The breakdown of this scaling occurs due to merging of the inner and outer mixing layers resulting in ambient fluid being mixed into the inner jet and or the transition from shear-like mixing layers to wake-like mixing layers. In addition, for the present configurations no effect of diameter ratio or confinement was found. Increasing the jet Reynolds number was found to decrease the distance between the jet exit and the start of outer shear layer growth resulting in much shorter outer jet lengths. This decrease in the outer jet length caused the stoichiometric mixing lengths to grow due do to the

increased amounts of ambient fluid being mixed into the center jet. Additional work is needed to understand buoyancy effects on L_S and when buoyancy effects becomes significant.

Acknowledgments

This work is supported by the NASA Constellation University Institutes Program (CUIP) under grant NCC3-989 jointly funded by NASA and DOD, with Claudia Meyer as the project manager.

References

[1]Champagne, F. H. and Wygnanski, I. J., "An Experimental Investigation of Coaxial Turbulent Jets," *International Journal of Heat and Mass Transfer*, Vol. 14, 1971, pp. 1445–1464.

[2]Durao, D. and Whitelaw, J. H., "Turbulent Mixing in the Developing Region of Coaxial Jets," *Transactions of the ASME: Journal of Fluids Engineering*, Vol. 95, 1973, pp. 467–473.

[3]Ribeiro, M. M. and Whitelaw, J. H., "Turbulent Mixing of Coaxial Jets with Particular Reference to the Near-Exit Region," *Transactions of the ASME: Journal of Fluids Engineering*, Vol. 98, 1976, pp. 284–291.

[4]Dahm, W. J. A., Frieler, C. E., and Tryggvason, G., "Vortex Structure and Dynamics in the Near Field of a Coaxial Jet," *Journal of Fluid Mechanics*, Vol. 241, 1992, pp. 371–402.

[5]Ribeiro, M. M. and Whitelaw, J. H., "Coaxial Jets with and without Swirl," *Journal of Fluid Mechanics*, Vol. 96, 1980, pp. 769–795.

[6]KO, N. W. M. and KWAN, A. S. H., "The Inital Region of Subsonic Coaxial Jets," *Journal of Fluid Mechanics*, Vol. 73, 1976, pp. 305–332.

[7]KWAN, A. S. H. and KO, N. W. M., "The Inital Region of Subsonic Coaxial Jets. Part 2," *Journal of Fluid Mechanics*, Vol. 82, 1977, pp. 273–287.

[8]Favre-Marinet, M. and Schettini, E. B. C., "The Density Field of Coaxial Jets with Large Velocity Ratio and Large Density Differences," *International Journal of Heat and Mass Transfer*, Vol. 44, 2001, pp. 1913–1924.

[9]Favre-Marinet, M., Camano, E. B., and Sarboch, J., "Near-Field of Coaxial Jets with Large Dendity Difference," *Experiments in Fluids*, Vol. 26, 1999, pp. 97–106.

[10]Tacina, K. M. and Dahm, W. J. A., "Effects of Heat Release on Turbulent Shear Flows. Part 1. A General Equivalence Principle for Non-Buoyant Flows and it's Application to Turbulent Jet Flames," *Journal of Fluid Mechanics*, Vol. 415, 2000, pp. 23–44.

[11]Dahm, W. J. A., "Effects of Heat Release on Turbulent Shear Flows. Part 2. Turbulent Mixing Layers and the Equivalence Principle," *Journal of Fluid Mechanics*, Vol. 540, 2005, pp. 1–19.

[12]Dahm, W. J. A. and Mayman, A. G., "Blowout limits of Turbulent Jet Diffusion Flames for Arbitrary Source Conditions," *AIAA Journal*, Vol. 28, No. 7, 1990, pp. 1157–1162.

[13]Murakami, E. and Papamoschou, D., "Mean Flow Development in Duel-Stream Compressible Jets," *AIAA Journal*, Vol. 40, No. 6, 2002, pp. 1131–1138.

[14]Dimotakis, P. E., "Two-Dimensional Shear-Layer Entrainment," *AIAA Journal*, Vol. 24, No. 11, 1986, pp. 1791–1796.

[15]Villermaux, E. and Rehab, H., "Mixing in Coaxial Jets," *Journal of Fluid Mechanics*, Vol. 425, 2000, pp. 161–185.

[16]Rehab, H., Villermaux, E., and Hopfinger, E. J., "Flow Regimes of Large-Velocity-Ratio Coaxial Jets," *Journal of Fluid Mechanics*, Vol. 345, 1997, pp. 357–381.

[17]Schumaker, S. A. and Driscoll, J. F., "Rocket Combustion Properties for Coaxial Injectors Operated at Elevated Pressures," AIAA 06–4704, AIAA 42^{nd} Joint Propulsion Conference, July 9–12, 2006.

[18]Moser, M. D., Merenich, J. J., Pal, S., and Santoro, R. J., "OH-Radical Imaging and Velocity Field Measurements in a Gaseous Hydrogen/Oxygen Rocket," AIAA 93–2036, AIAA 29^{th} Joint Propulsion Conference, June 28-30, 1993.

[19]Santoro, R. J., Pal, S., and Woodward, R. D., "Rocket Testing at University Facilities," AIAA 01–0748, AIAA 39^{th} Aerospace Sciences Meeting, January 8-11, 2001.

[20]Hutt, J. J. and Cramer, J. M., "Advanced Rocket Injector Development at the Marshall Space Flight Center," AIAA 96–4266, AIAA Space Programs and Technologies Conference, September 24–26, 1996.

[21]Lozano, A., Yip, B., and Hanson, R. K., "Acetone: a Tracer for Concentration Measurments in Gaseous Flows by Planar Laser-Induced Fluorescence," *Experiments in Fluids*, Vol. 13, 1992, pp. 369–376.

[22]Yuen, L. S., Peters, J. E., and Lucht, R. P., "Pressure Dependence of Laser-Induced Fluorescence from Acetone," *Applied Optics*, Vol. 36, No. 15, 1997, pp. 3271–3277.

[23]Thurber, M. C. and Hanson, R. K., "Pressure and Composition Dependences of Acetone Laer-Induced Fluorescence with excitation at 248, 266, 308nm," *Applied Physics B*, Vol. 69, 1999, pp. 229–240.

[24]van Cruyningen, I., Lozano, A., and Hanson, R. K., "Quantitative Imaging of Concentration by Planar Laser-Induced Fluorescence," *Experiments in Fluids*, Vol. 10, 1990, pp. 41–49.

[25]Clemens, N. T., *Encyclopedia of Imaging Science and Technology*, chap. Flow Imaging, John Wiley and Sons, New York, 2002, pp. 390–419.

[26]Warda, H. A., Kassab, S. Z., Elshorbagy, K. A., and Elsaadawy, E. A., "An experimental Investigation of the Near-Field Region of a Free Turbulent Coaxial Jet using LDA," *Flow Measurement and Instrumentation*, Vol. 10, 1999, pp. 15–26.

[27]HIll, B. J., "Measurment of Local Entrainment Rate in The Initial Region of Axisymmetric Turbulent Air Jets," *Journal of Fluid Mechanics*, Vol. 51, 1972, pp. 773–779.

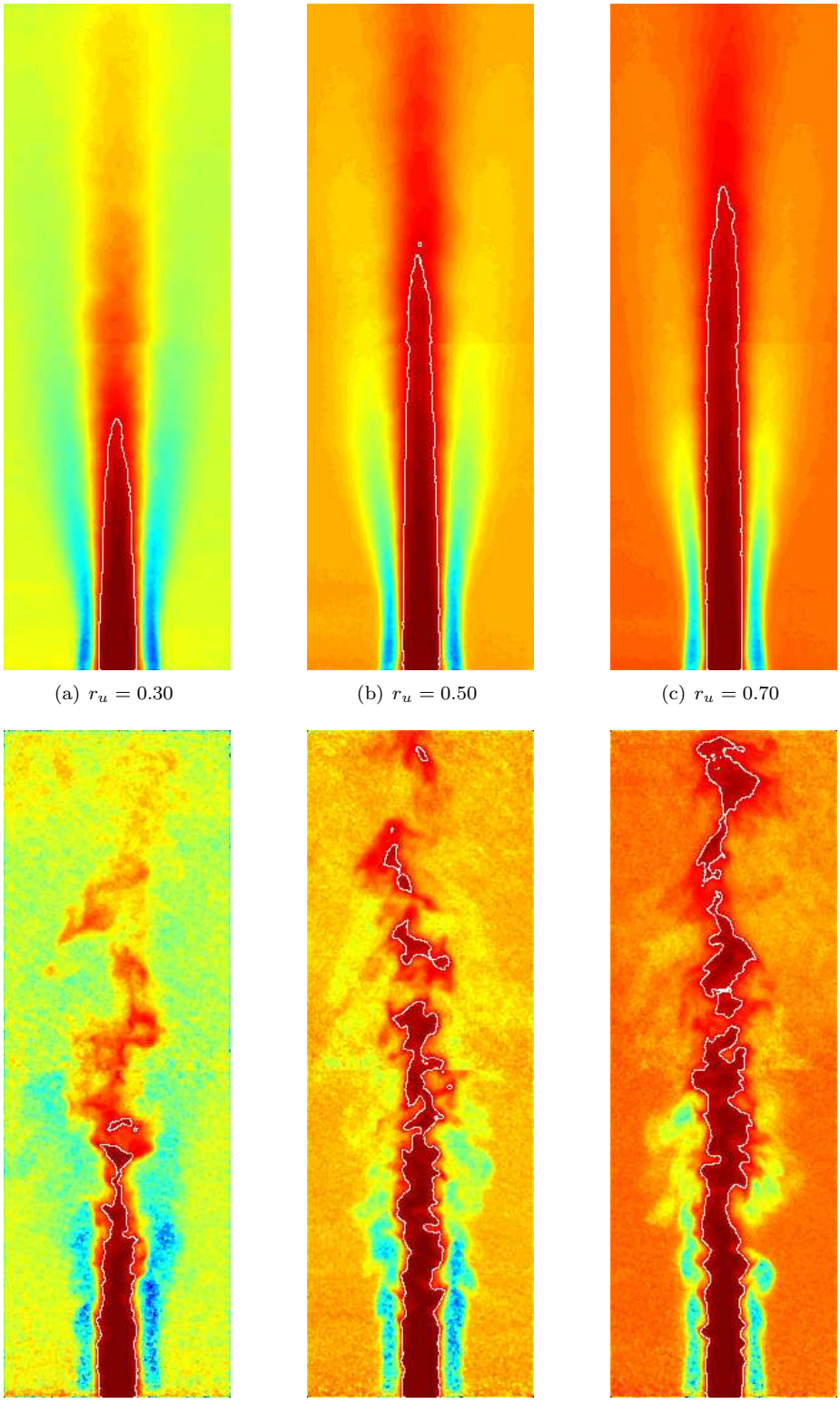

(a) $r_u = 0.30$ (b) $r_u = 0.50$ (c) $r_u = 0.70$

(d) $r_u = 0.30$ (e) $r_u = 0.50$ (f) $r_u = 0.70$

Figure 8. Average a)-c)and instantaneous d)-f) mixture fraction fields of air/H_2 coaxial jets for $r_u = 0.30, 0.50, 0.70$, data group G5. White line marks stoichiometric contour, $f_s = 0.89$.

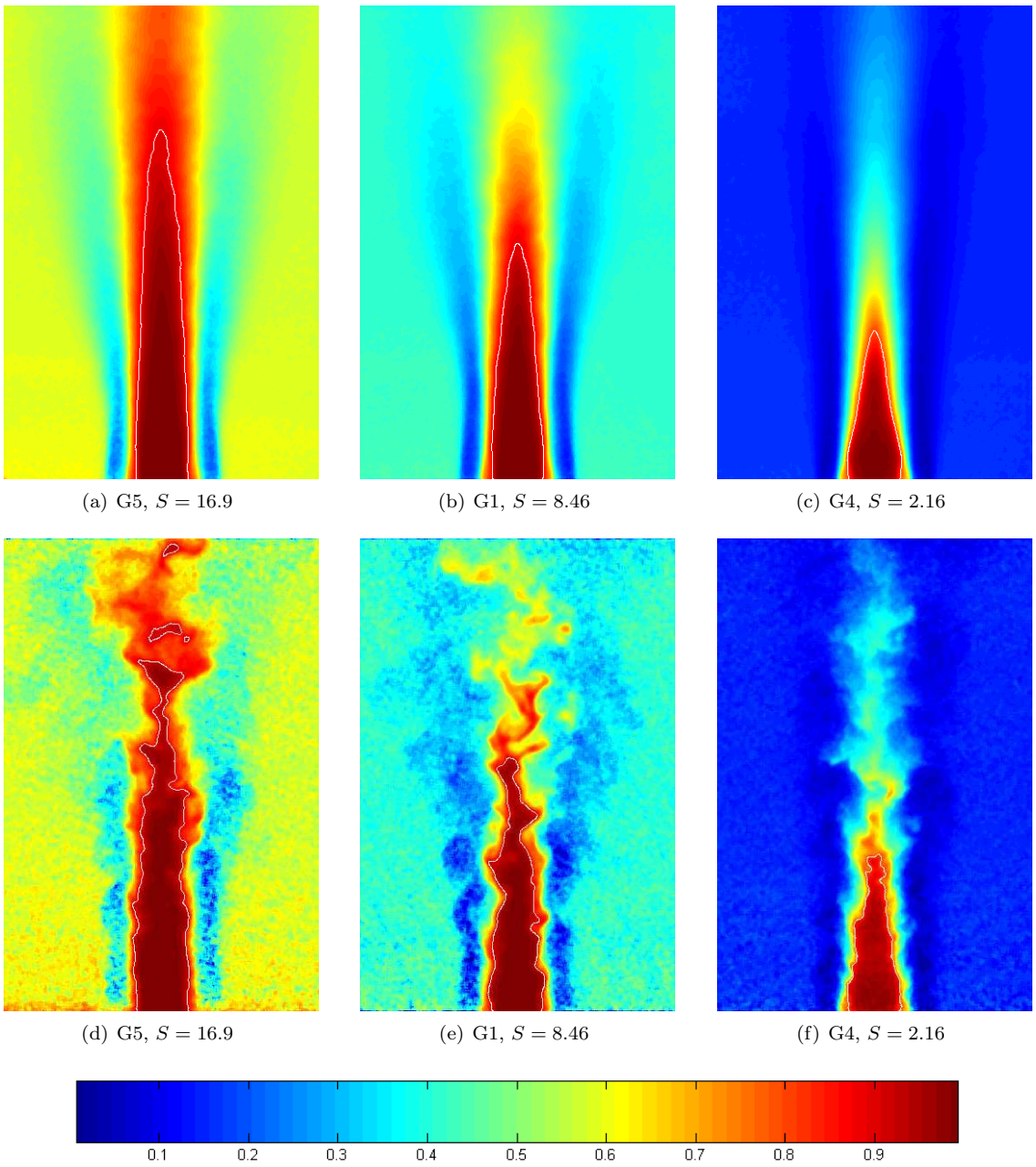

(a) G5, $S = 16.9$ (b) G1, $S = 8.46$ (c) G4, $S = 2.16$

(d) G5, $S = 16.9$ (e) G1, $S = 8.46$ (f) G4, $S = 2.16$

Figure 9. Average a)-c)and instantaneous d)-f) mixture fraction fields for $r_u = 0.30$. White line marks stoichiometric contour. a)-b) and d)-e) $f_s = 0.89$. c) and f) $f_s = 0.80$

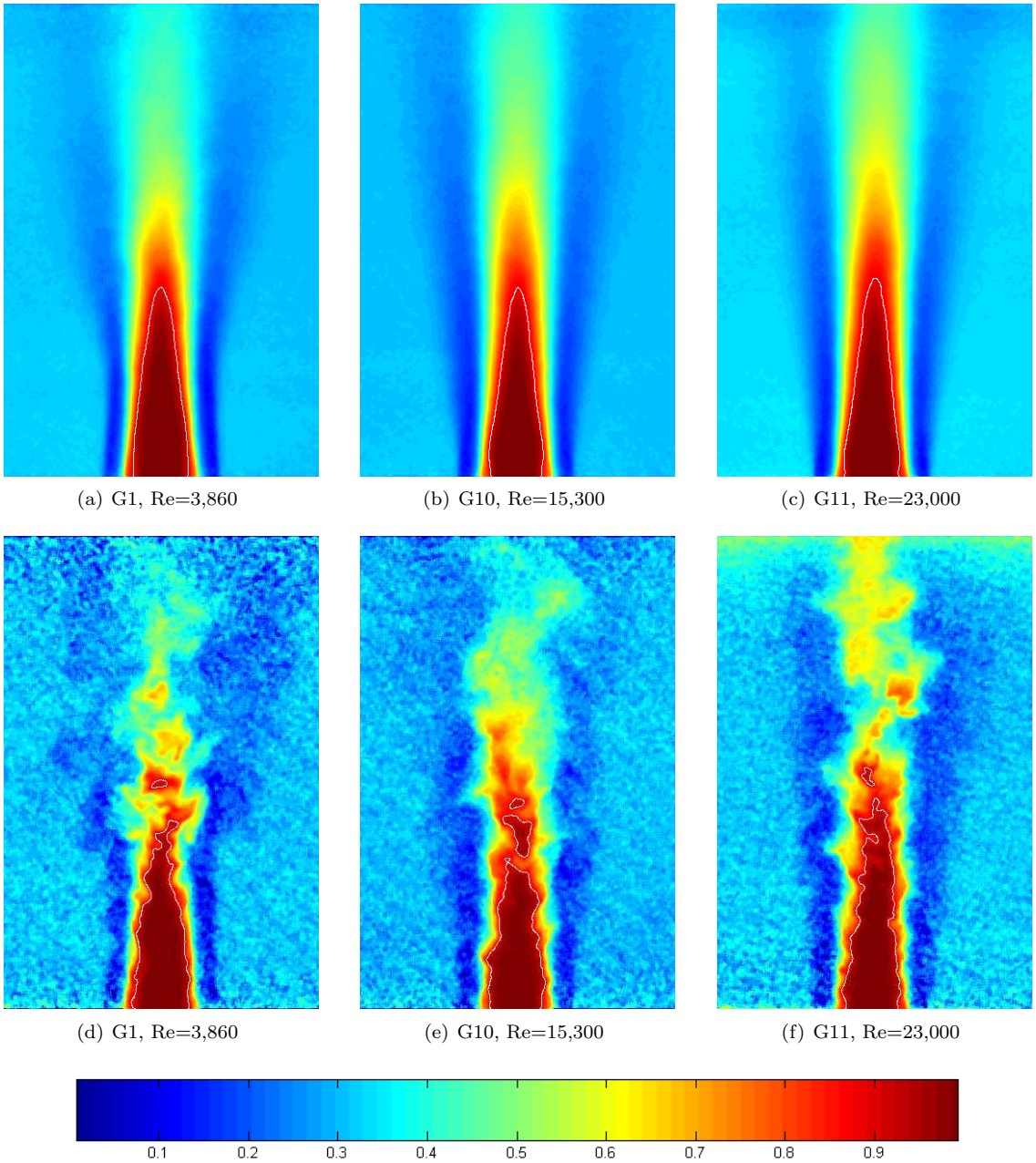

(a) G1, Re=3,860 (b) G10, Re=15,300 (c) G11, Re=23,000

(d) G1, Re=3,860 (e) G10, Re=15,300 (f) G11, Re=23,000

Figure 10. Average a)-c)and instantaneous d)-f) mixture fraction fields of He-air coaxial jets for $r_u = 0.20$ with varying Reynolds number. White line marks stoichiometric contour, $f_s = 0.89$.

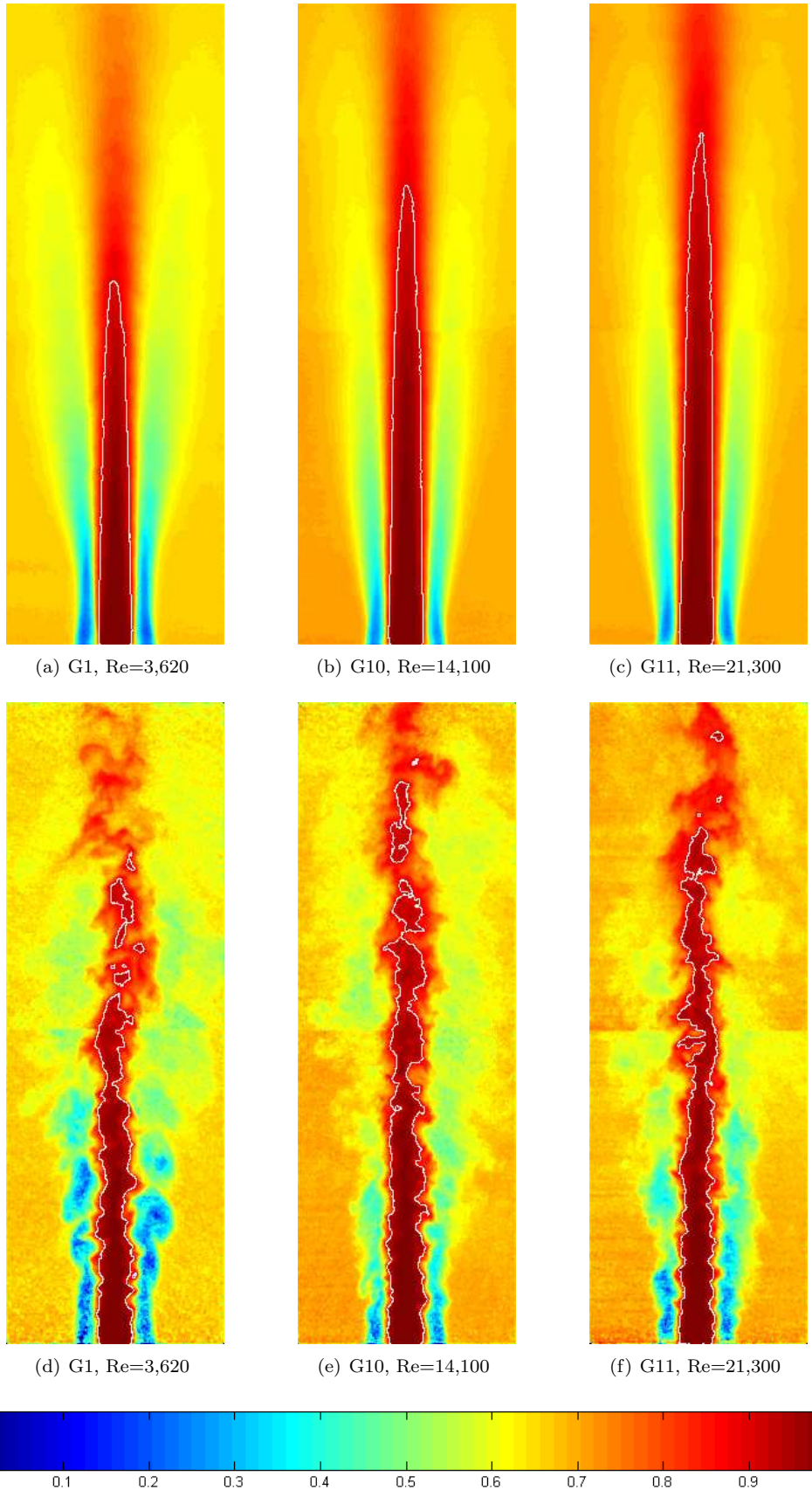

(a) G1, Re=3,620 (b) G10, Re=14,100 (c) G11, Re=21,300

(d) G1, Re=3,620 (e) G10, Re=14,100 (f) G11, Re=21,300

Figure 11. Average a)-c)and instantaneous d)-f) mixture fraction fields of air/He coaxial jets for $r_u = 0.90$ with varying Reynolds number. White line marks stoichiometric contour, $f_s = 0.89$.